Langmuir

ARTICLE

pubs.acs.org/Langmuir

kT-Scale Colloidal Interactions in High Frequency Inhomogeneous AC Electric Fields. I. Single Particles

Jaime J. Juárez, Jing-Qin Cui, Brian G. Liu, and Michael A. Bevan*

Chemical and Biomolecular Engineering, Johns Hopkins University, Baltimore, Maryland 21286, United States

ABSTRACT: We report nonintrusive optical microscopy measurements of single micrometer-sized silica and polystyrene colloids in inhomogeneous AC electric fields as a function of field amplitude and frequency. By using a Boltzmann inversion of the time-averaged sampling of single particles within inhomogeneous electric fields, we sensitively measure induced dipole−field interactions on the kT energy scale and fN force scale. Measurements are reported for frequencies when the particle polarizability is greater and less than the medium, as well as the crossover between these conditions when dipole−field interactions vanish. For all cases, the measured interactions are well-described by theoretical potentials by fitting a nondimensional induced dipole−field magnitude. While silica dipole−field magnitudes are well-described by existing electrokinetic models, the polystyrene results suggest an anomalously high surface conductance. Sensitive measurements of dipole−field interactions in this work provide a basis to understand dipole−dipole interactions in particle ensembles in the same measurement geometry in part II.

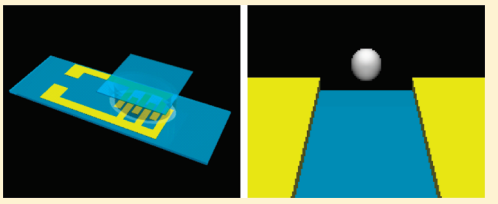

INTRODUCTION

The interaction of induced dipoles on colloidal particles with inhomogeneous high-frequency AC electric fields has been the subject of many scientific studies[1−3] and has been developed for use in numerous technological applications.[4,5] Such dipole−field interactions are most commonly associated with dielectrophoresis, which refers to the transport process arising from a conservative force operating on induced dipoles in inhomogeneous electric fields in opposition to dissipative hydrodynamic forces. Applications have traditionally focused on large-scale particle separations, whereas emerging technologies are increasingly focused on manipulation, characterization, and sorting of individual particles.[5]

Much of the scientific basis for understanding induced dipole−inhomogeneous electric field interactions is well-established. However, some issues remain with modeling the contributions of electrical double layers (EDL) for dielectric colloids with charged surfaces in aqueous media.[6−10] Many of the issues surrounding the EDL contribution are based on finding models that capture the frequency dependent dipole−field magnitude and direction for different material systems. Much of the effort has focused on determining colloid surface conductances based on electrokinetic models valid for a range of particle and EDL dimensions and physicochemical surface properties. Although some analytically simple models have become favored for modeling forces involved in dielectrophoretic transport,[11] it is not clear that such approaches are satisfactory for first-principles predictions of dipole−field interactions.

In the present study, our goal is to directly and sensitively measure and model the interaction potential between single induced dipoles and inhomogeneous electric fields. By knowing weak electric field mediated interactions on the order of the thermal energy kT (and femtonewton (fN) force scale), such interactions can be manipulated in an informed manner to minimally and constructively perturb equilibrium colloidal self-assembly processes.[12−14] In terms of precedent, previous studies have observed trapping of many particles (e.g., cells[15] and colloids[16,17]) within energy wells due to dipole−field interactions, but these studies did not attempt to measure single or ensemble dipole−field interactions. One study measured the frequency dependent behavior of single colloids using a force-transducer based optical tweezer measurement,[18] but the effective trap spring constant limited these measurements to ∼piconewton (pN) force resolution. Although numerous studies have quantified interactions of induced dipoles with inhomogeneous electric fields as part of dielectrophoresis measurements, the authors are not aware of any study that has measured single dipole−field interactions on the kT-scale with relevance to colloidal assembly processes.

In the following, we describe a new optical microscopy method to measure the dipole−field interaction for single silica and polystyrene (PS) colloids as a function of particle size and electric field amplitude and frequency. Our approach is based on nonintrusive observation of the time-averaged equilibrium sampling of single colloids in inhomogeneous electric fields formed between coplanar thin film electrodes on microscope slides (see Figure 1). We have used this approach to measure other colloidal forces[19] and once before to measure single-sized silica particles interacting with an electric field at a single amplitude and frequency.[14] A simple Boltzmann inversion of the measured histograms yields the single particle potential energy vs position within the electric field. The equilibrium nature of these

Received: April 21, 2011
Revised: June 14, 2011
Published: June 15, 2011

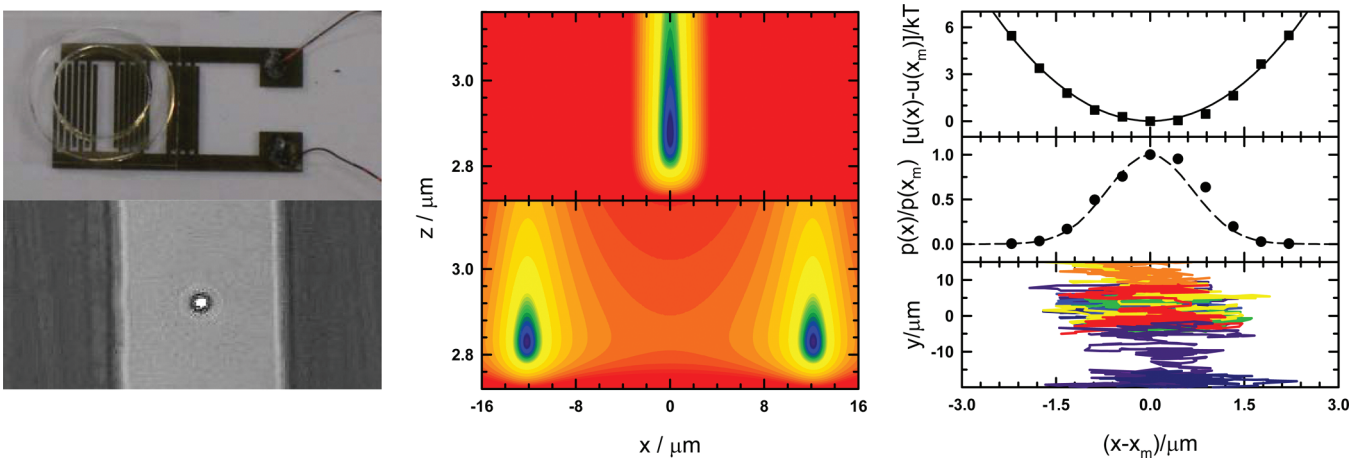

Figure 1. Schematics related to single particle measurement configuration. (left, a) Actual device top view of experimental cell showing microfabricated electrode and wires, PDMS O-ring, and coverslip sealed with vacuum grease, and image from video microscopy movie of single SiO_2 colloid ($2a$ = 3.01 μm) diffusing within electrode gap for $f_{CM} < 0$ case. (middle, b) Cross-sectional (i.e., XZ) view of net potential energy $[u(x, z) - u(x_r, z_r)]$ resulting from the superposition of contributions from the underlying microscope slide, gravity, and the inhomogeneous electric field within the 30 μm coplanar, thin film electrode gap. Log spectrum energy scale (0.01−10 kT) shows results for a single PS colloid ($2a$ = 5 μm) in a 300 mV AC electric field at 1 MHz (top) and 360 kHz (bottom) for the parameters in Tables 3 and 4. (right, d) Trajectory of single SiO_2 ($2a$ = 3.01 μm) colloid in a 2 V, 1 MHz AC electric field captured using video microscopy (linear spectrum time scale, 0−30 min) used to construct a histogram that is inverted with Boltzmann's equation to obtain a potential energy profile.

measurements inherently provides a measure of kT-scale interactions without contributions from dissipative hydrodynamic forces (encountered in transport measurements). In all cases, we are able to fit a nondimensional dipole−field magnitude to the measured potential energy profiles, which we then compare against available analytically simple electrokinetic models. We then use these measured dipole−field interactions to interpret dipole−dipole interactions in particle ensembles in Part II.[20]

THEORY

The net potential energy of single colloidal particles in a nonuniform electric field near a planar wall surface is the sum of particle−wall and particle−field interactions given by

$$u^{net}(x,z) = u^{pw}(z) + u^{pf}(x,z) \quad (1)$$

where x is the position within the electrode gap relative to the center, and $z = h + a$ where h is the particle−wall surface-to-surface separation and $2a$ is the particle diameter.

The net particle−surface interaction in the limit of negligible van der Waals includes only electrostatic interactions given by[21]

$$u^{pw}(z) = u_e^{pw}(z) \quad (2)$$

where

$$u_e^{pw}(z) = B^{pw}\, exp[-\kappa(z-a)] \quad (3)$$

$$B^{pw} = 64\pi\varepsilon_m a\left(\frac{kT}{z_v e}\right)^2 tanh\left(\frac{z_v e\psi_p}{4kT}\right) tanh\left(\frac{z_v e\psi_w}{4kT}\right) \quad (4)$$

where κ^{-1} is the Debye length, ε_m is the medium dielectric constant, k is Boltzmann's constant, T is absolute temperature, e is the charge of an electron, z_v is the electrolyte valence, and ψ_p and ψ_w are the particle and wall electrostatic surface potentials.

The net particle−field interaction includes the gravitational potential energy and the interaction of induced dipoles with electric field gradients as

$$u^{pf}(x,z) = u_g^{pf}(z) + u_{de}^{pf}(x,z) \quad (5)$$

where the gravitational potential energy is given by

$$u_g^{pf}(z) = Gz \quad (6)$$

where $G = (4/3)\pi a^3(\rho_p - \rho_m)g$ is the buoyant particle weight, ρ_p and ρ_m are the particle and medium densities, and g is acceleration due to gravity.

The interaction of an induced dipole with a nonuniform electric field for the geometry in Figure 1 is[22]

$$u_{de}^{pf}(x,z) = -2kT\lambda f_{cm}^{-1}E^*(x,z)^2 \quad (7)$$

where $E^*(x, z) = E(x, z)/E_0$ is the local normalized electric field from our previous paper,[14] $E_0 = 8^{-0.5}V_{pp}/d_g$, V_{pp} is the applied peak-to-peak voltage, d_g is the distance between electrodes, and λ is the relative dipolar and Brownian energies given by[23]

$$\lambda = \pi\varepsilon_m a^3(f_{cm}E_0)^2/kT \quad (8)$$

and f_{cm} is the Clausius-Mosotti factor given as

$$f_{cm} = Re[(\tilde{\varepsilon}_p - \tilde{\varepsilon}_m)/(\tilde{\varepsilon}_p + 2\tilde{\varepsilon}_m)] \quad (9)$$

where $\tilde{\varepsilon}_m$ and $\tilde{\varepsilon}_p$ are complex particle and medium permittivities of the form

$$\tilde{\varepsilon} = \varepsilon - i\sigma/\omega \quad (10)$$

where σ is conductivity, and ω is angular frequency. The crossover frequency, ω_c, corresponding to the transition between negative and positive values of f_{cm} is given as (by letting $f_{cm} = 0$ in eq 9)

$$\omega_c = \left[\frac{(\sigma_p - \sigma_m)(\sigma_p + 2\sigma_m)}{(\varepsilon_m - \varepsilon_p)(\varepsilon_p + 2\varepsilon_m)}\right]^{1/2} \quad (11)$$

dx.doi.org/10.1021/la201478y |Langmuir 2011, 27, 9211–9218

For dielectric particles, the particle conductivity is given by[11]

$$\sigma_p = 2K_n a^{-1} \quad (12)$$

where K_n is the surface conductance for thin electrostatic double layers ($\kappa\alpha \gg 1$) given by[24]

$$K_n = \left[4(1+m)\kappa^{-1}\, sinh^2\left(\frac{ze\zeta}{4kT}\right) + 2m\beta^{-1}\, sinh^2\left(\frac{ze\zeta}{2kT}\right)\right]\sigma_m \quad (13)$$

where ζ is the particle zeta potential, β^{-1} is a slip length, and m is a nondimensional ionic drag coefficient given by

$$m = \frac{2\varepsilon_m}{\eta D}\left(\frac{kT}{ze}\right)^2 \quad (14)$$

where η is the medium viscosity, and D is the diffusivity of the ion with the highest charge.[25,26] In the absence of slip, eq 13 reduces to the usual expression for surface conductance.[10,26]

For noninteracting colloids approaching infinite dilution, the probability of sampling different positions within the electrode gap can be related to the relative potential energies of different positions from eq 1 using Boltzmann's equation as[27]

$$p(x,z) = p(x_r,z_r)\, exp\left[-\left(u^{net}(x,z) - u^{net}(x_r,z_r)\right)/kT\right] \quad (15)$$

where x_r and z_r are reference coordinates that determine the relative potential energy. Equation 15 can be inverted to obtain relative potential energies from measured histograms as

$$\frac{u^{net}(x,z) - u^{net}(x_r,z_r)}{kT} = ln\left[p(x_r,z_r)/p(x,z)\right] \quad (16)$$

When excursions normal to the surface in the z direction cannot be measured, the effective probability distribution projected onto the x dimension can be obtained by integrating over z as

$$p(x) = (z_u - z_l)^{-1}\int_{z_l}^{z_u} p(x,z)\, dz \quad (17)$$

which can be used to obtain the effective potential in the x direction as

$$\frac{u^{net}(x) - u^{net}(x_r)}{kT} = ln\left[p(x_r)/p(x)\right] \quad (18)$$

MATERIALS AND METHODS

Coplanar gold film electrodes were patterned on glass microscope slides (75 mm × 25 mm × 1 mm, Corning) that were washed with acetone (Sigma-Aldrich), KOH (Sigma-Aldrich), and deionized water prior to patterning. Electrode patterns were obtained by spin-coating photoresist (SU-8, Microchem) onto microscope slides, UV exposure through a chrome photomask, and vapor deposition of 50 nm gold films in ~330 μm strips separated by ~30 μm. Nominal 1.59 μm, 2.34 μm, and 3.01 μm silica colloids (Bangs Laboratories) and nominal 3 μm, 4 μm, and 5 μm sulfate stabilized PS colloids (Invitrogen) were dispersed in deionized water and allowed to sediment for 30 min in a polydimethylsiloxane (Dow Chemical) batch cell (1 mm high × 5 mm diameter) sealed with a coverslip (Corning). The coplanar electrode device was connected in series with a function generator (Agilent, 33220A) to generate AC electric fields. Optical microscopy experiments were performed using an inverted microscope (Zeiss) and a 63× objective. Videos were captured at 28 frames/s and an image size of 336 pixels × 256 pixels (129 μm × 98 μm) with a charge coupled device camera (Hamamatsu, Orca-ER) and *Streampix* (Norpix) acquisition software. Particle locations and trajectories were obtained in sets of 30 000 images using standard algorithms coded in FORTRAN.[28]

RESULTS AND DISCUSSION

Single Particle Measurement Configuration. To measure single, micrometer-sized colloids interacting with inhomogeneous, high-frequency AC electric fields, we perform measurements in between coplanar, gold film gold electrode gaps patterned on glass microscope slides as shown in Figures 1a.[14,29] In this geometry, dilute ensembles of micrometer-sized colloids can be levitated above the gold and glass regions of the patterned microscope slide surface. Specifically, electrostatic repulsion is sufficiently long-range for a combination of moderate surface potentials (>10 mV) and low ionic strengths (~0.1 mM) that van der Waals attraction does not produce irreversible deposition of colloids onto either the glass or gold regions (based on our previous direct measurements[27]). To clarify the measurement geometry, Figure 1a also shows a CCD camera image of a single levitated 2.34 μm silica colloid in a 1 MHz AC electric field in the electrode gap.

In the absence of an electric field, electrostatic repulsion between the colloid and the underlying substrate (eq 3) are balanced by gravitational potential energy (eq 6) that cause the particle to be levitated at a mechanical equilibrium (i.e., potential energy minimum) height, $h_m = \kappa^{-1}\ln(\kappa B^{pw}/G)$.[30] Excursions normal to the substrate about the mechanical equilibrium position are on the order of several hundred nanometers as determined by the Boltzmann distribution (eq 15) due to the confining potential energy well (the z component of eq 1).[31] There is essentially no restriction to lateral diffusion over the gold and glass regions of the surface in the absence of an electric field.[27]

In the presence of high-frequency AC electric fields between the gold film electrodes, in addition to electrostatic and gravitational interactions, the field induces dipoles on colloids, which interact with electric field gradients. At high frequencies, the particles are less polarizable than the medium, which corresponds to $f_{CM} < 0$ in eq 7, and at lower frequencies below the crossover frequency (i.e., eq 11), particles can become more polarizable than the surrounding medium, which corresponds to $f_{CM} > 0$ in eq 7. As shown in Figure 1b, depending on the sign of f_{CM}, induced dipoles experience their lowest potential energy either where the field magnitude is lowest in the gap center (i.e., $f_{CM} < 0$) or highest at the electrode edges (i.e., $f_{CM} > 0$). When induced dipoles migrate in inhomogeneous electric fields and are balanced by hydrodynamic drag, the resulting transport mechanism is termed "dielectrophoresis". When $f_{CM} < 0$, this transport is referred to as "negative dielectrophoresis", and when $f_{CM} > 0$, it is called "positive dielectrophoresis". In this work, we are interested in static interactions (rather than phoretic transport), so we simply refer to these two cases as the "negative f_{CM}" and "positive f_{CM}" cases.

In the presence of an electric field, but absence of other surface or body forces (see Figure 1b): (1) the lateral mechanical equilibrium position is either $x_m = 0$ (i.e., the gap center) in the negative f_{CM} case or $x_m = \pm d_g/2$ (i.e., the electrode edges) in the positive f_{CM} case, and (2) electric field gradients normal to the surface in the z direction either lift the particle away from the surface in the negative f_{CM} case or push it into contact with the

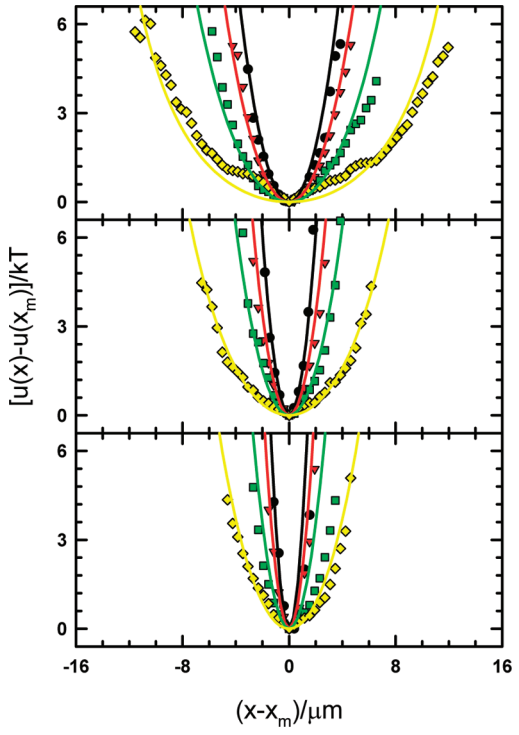

Figure 2. Interactions of different-sized SiO_2 colloids with inhomogeneous AC electric field in 30 μm electrode gap for 1 MHz frequency and amplitudes of 0.5 V (yellow diamond), 1.0 V (green square), 1.5 V (red triangle), and 2 V (black circle). Nominal particles sizes of 1.59 μm (top), 2.34 μm (middle), and 3.01 μm (bottom) were each measured at the same field conditions. Potential energy profiles were fit using eqs 1−7 with parameters reported in Table 1. Separation and energy scales are referenced to their values at the electrode gap midpoint.

wall at $h_m = 0$ in the positive f_{CM} case. In the presence of surface forces, gravity, and electric field mediated interactions, a 2D potential energy space in the z and x directions as shown in Figure 1b (for both cases) causes single particles to sample different positions with probabilities given by eqs 15 and 16. Although Figure 1b shows a 2D potential energy space, the strong forces (large potential energy gradient) in the z direction confine the particles within a several hundred nanometer range normal to the surface. As a result, evaluating eq 16 at the most probable height, h_m (or $z_m = h_m + a$), is essentially identical to eq 18, which shows excursions normal to the substrate can be ignored in the analysis.

In the following, we nonintrusively probe this 2D potential energy space with single colloids as a function of field amplitude and frequency by monitoring their trajectories in the x and y directions as shown in Figure 1c, which we use to build histograms in the x direction since there is no y dependence. These measured histograms are then inverted (i.e., eq 18) to obtain potentials for comparison with eq 1 evaluated at $z_m = h_m + a$. This yields kT-scale measurements of the frequency dependence of the interactions between induced dipoles and high-frequency inhomogeneous AC electric fields, which has not been previously measured on this energy scale (and corresponding force scales).

Dipole-Field Interaction vs AC Field Amplitude. In Figure 2, we first measure the amplitude dependence of the dipole−field interaction for the negative f_{CM} case at fixed frequency (i.e., 1 MHz) as a function of particle size. Results are presented for silica colloids with nominal diameters of $2a$ = 1.59 μm, 2.34 μm, and 3.01 μm in deionized water with no added electrolyte. Silica colloids were chosen for these measurements because their high buoyant weight allows them to stay near the microscope slide in the presence of significant upward forces that can move lighter latex colloids away from the microscope slide. For each particle size, field amplitudes were investigated for applied voltages of 0.5−2 V (used in the analytical expression for the electric field, $E^*(x, z) = E(x, z)/E_0$, in eq 7 as given in our previous paper[14]). In each plot, points correspond to potentials obtained from a Boltzmann inversion of measured particle histograms (i.e., eq 18), and lines correspond to potentials obtained by fitting eq 1 to the points using λ/f_{CM} in eq 7 as the only adjustable parameter for each particle size. Although λ contains f_{CM}, so that they are not independent, we discuss both quantities; λ is the nondimensional dipole−field strength and f_{CM} captures the material properties. Table 1 lists all other parameters used for the theoretical profiles in Figure 2, which were obtained from independent measurements or literature results.

Table 1. Parameters Used to Fit eqs 1−7 to Measured Potential Energy Profiles for the Silica-Amplitude Results in Figure 2[a]

parameter	equation	value
$2a$ (μm)[b]	3, 4, 6, 8, 12	1.59, 2.34, 3.01
$\varepsilon_m/\varepsilon_0$[c]	4, 8-11, 14,	78
κ^{-1} (nm)[d]	3, 13	30
$\zeta_p = \psi_p = \psi_w$ (mV)[e]	4, 13	−75
ρ_p (g/cm^3)[c]	6	1.96
ρ_m (g/cm^3)[c]	6	1
V_{pp} (V)[f]	7	0.5, 1, 1.5, 2
d_g (μm)[g]	7	33
$\omega/2\pi$ (kHz)[f]	10	1000
λ_{fit}/V_{pp}^2 ($1/V^2$)	8	**3.2, 13.0, 32.5**
f_{CM}[c]	7, 8	−0.457, −0.46, −0.462

[a] The nondimensional dipole−field magnitude, λ, was the only adjustable parameter (shown in bold). [b] Parameter fixed using nominal manufacturer particle sizes. [c] Parameter fixed using handbook values.[38] [d] Parameter fixed using estimate from previous diffusion measurements.[14] [e] Parameter fixed using estimate from previous direct measurements.[31−33] [f] Parameter fixed using function generator input. [g] Parameter fixed by measuring with optical microscopy.

The measured and fit potentials display excellent agreement in all cases except for a minor deviation in the measurements at the lowest applied voltage. In particular, the functional form of the predicted dipole−field interactions (i.e., eq 7) accurately captures the directly measured potentials on the kT energy and fN force scales. This provides unprecedented resolution for direct measurements of single particles interacting with inhomogeneous, high-frequency AC electric fields. This provides a robust foundation for manipulating such interactions in self- and directed-assembly processes and more generally in a variety of soft matter applications.

An extra feature in the measured potentials becomes apparent at the lowest applied voltage of 0.5 V and becomes more prominent as the particle size decreases. It should be noted that this feature was qualitatively reproducible in ten separate measurements in the 1.59 μm/0.5 V case, although there were quantitative variations. Because this feature appears for

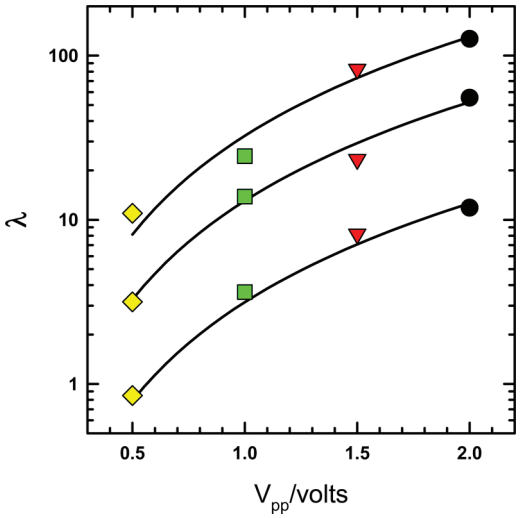

Figure 3. Values of λ vs V_{pp} obtained by fitting eqs 1−7 to measured potential energy profiles in Figure 2. The symbols shapes and colors are the same as in Figure 2. Curve fits for each particle size are obtained using eqs 8−14 with parameters reported in Table 2. Curves and associated points correspond to particle diameters of 1.59 μm (bottom), 2.34 μm (middle), and 3.01 μm (top).

Table 2. Parameters Used to Fit eqs 8−14 to Measured λ Values for the Silica-Amplitude Results in Figure 3[a]

parameter	equation	value
$\varepsilon_p/\varepsilon_0$[b]	9	3.8
D (10^{-9} m^2 s^{-1})[b]	14	1.3
η (Pa−s)[b]	14	8.9×10^{-4}
m[c]	13	0.79
β^{-1} (nm)[d]	13	0
σ_m(μS/cm)	10, 11, 13	**13.0**
K_n (nS)[c]	12	0.089
$\omega_C/2\pi$ (kHz)[c]	11	- -
$\lambda_{fit}/\lambda_{predicted}$	- -	0.75, 0.8, 0.88

[a] The medium conductivity, σ_m, was the only adjustable parameter (shown in bold). [b] Parameter fixed using handbook values.[38] [c] Parameter fixed using equations. [d] Parameter set equal to zero.

decreasing voltage and particle size, it may arise from several effects associated with vanishing dipole−field interactions (at sub-fN resolution). For example, factors that might lead to this slight deviation could include contributions from electrode irregularities, limited statistical sampling of the very shallow/broad potential, or contributions from other electrokinetic effects that vanishes with a different dependence than the E^2 dipole−field interaction. The appearance of this feature in only the weakest interactions does not suggest a significant shortcoming of the theory in eq 7.

To further investigate whether the fits values of λ and f_{CM} in Figure 2 make sense with respect to relevant electrokinetic models, Figure 3 shows measured and predicted λ vs V_{pp} for each particle size. The curve fits to the λ values were obtained using eqs 8−14 using typical parameters estimates summarized in Table 2. In particular, a medium conductivity of σ_m = 13 μS/cm was used to be consistent with a 0.1 mM NaCl solution and the Debye length of κ^{-1} = 30 nm used to describe particle−wall

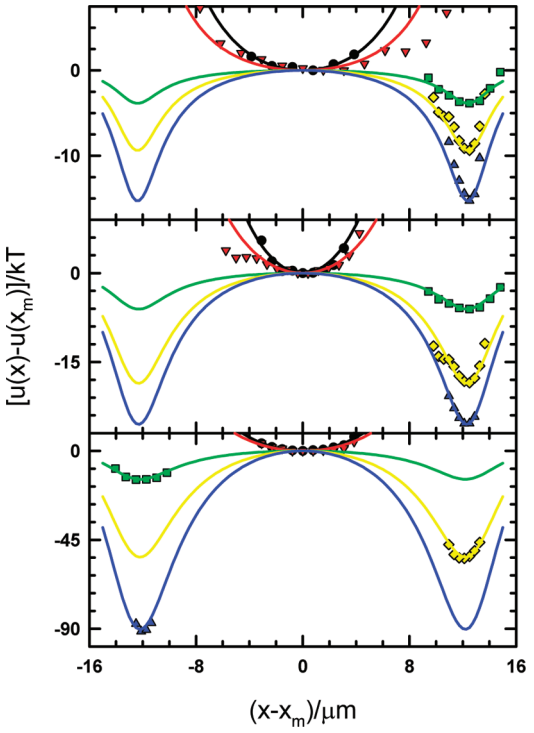

Figure 4. Interactions of different-sized PS colloids with inhomogeneous AC electric field in 30 μm electrode gap for an amplitude of V_{pp} = 300 mV and frequencies of 200 kHz (blue triangles), 300 kHz (yellow diamonds), 375 kHz (green squares), 500 kHz (red inverted triangles), and 1 MHz (black circles). Nominal particles sizes of 3 μm (top), 4 μm (middle), and 5 μm (bottom) were each measured at the same field conditions. Potential energy profiles were fit using eqs 1−7 with parameters reported in Table 3. Separation and energy scales are referenced to their values at the electrode gap midpoint.

electrostatic interactions in Figure 2. This value is consistent with conductivity probe measurements, although this is near the low end of what can be measured accurately with our commercial instrument. Choices for other material property values are described in Table 2.

The results in Figure 3 show that the potentials are consistent with model predictions within the uncertainty of measurements and estimated parameters. To obtain the curve fits in Figure 3, the fit values of λ are 75−90% of the values predicted from eqs 8−14 using reasonable estimates for all parameters reported in Table 2. However, in eq 8, the a^3 and E_0^2 dependence means that a 10% overestimate in particle size or 15% overestimate in the applied voltage in the microelectrode gap would easily account for this discrepancy. In fact, both the manufacturer's reported particle size and the applied voltage are both expected to be overestimates. The particle size mode we typically encounter in microscopy experiments (via in situ size measurements[31−33]) is usually less than the manufacturer's mean size. This is typical for asymmetric size distributions for micrometer-sized colloids where the mode is always less than the mean. The value of V_{pp} used in the calculation is read from a function generator as the voltage source, but losses are also expected to make this value smaller at the electrode gap (we do not have an in situ measure of the voltage difference across the 30 μm gap). In short, the difference between measured and predicted λ in Figure 3 can easily be accounted for by biases in both a^3 and E_0^2 contributions in eq 8.

dx.doi.org/10.1021/la201478y |*Langmuir* 2011, 27, 9211–9218

As a result, the predicted values of f_{CM} in eq 9 that contains all material properties that enter into λ in eq 8 are easily estimated using established electrokinetic models (eqs 10−14) with standard parameter estimates (Table 2). Because the discrepancy between measured and predicted λ can be explained by overestimates in a^3 and E_0^2, there is no need to explore more exotic models (e.g., surface slip term in eq 13) for the material properties that contribute to f_{CM}. Although we do not pursue an exhaustive parametric analysis including fitting procedures and independent measurements to obtain the values in Tables 1 and 2, the sensitive single particle measurements in Figure 2 are well described by existing theories for dipole−field interactions and electrokinetic models of the dipole formation.

The measured properties in conjunction with eq 11 indicate there is no crossover from $f_{CM} < 0$ to $f_{CM} > 0$ for these silica particles, which we confirmed in frequency-dependent measurements. Because the silica particle conductivity never exceeds the medium conductivity, it never becomes more polarizable than the medium. In all experimental tests for a crossover, AC electroosmosis[3] was encountered at frequencies below 100 kHz rather than a transition to a positive f_{CM} value.

Dipole−Field Interaction vs AC Field Frequency. With an understanding of amplitude-dependent interactions for the negative f_{CM} case at high frequencies, we now explore in Figure 4 frequency-dependent interactions of PS colloids at a fixed voltage. The results in Figure 4 now show potential measurements for cases involving both negative and positive values of f_{CM} as a function of PS particle size. The transition from negative to positive f_{CM} values (at ω_C in eq 11) appears as the particle−field interaction transitioning from a single well in the middle of the electrode gap to a double well potential with minima near the electrode edges.

Figure 4 shows results for sulfate-stabilized PS colloids with nominal diameters of $2a$ = 3 μm, 4 μm, and 5 μm in deionized water with no added electrolyte. The field amplitude was fixed with V_{pp} = 300 mV. In the experiments to generate the data in Figure 4, the AC field frequency was first varied in each experiment from 1 MHz down to 100 kHz in 100 kHz increments, and after detection of a crossover from negative to positive f_{CM}, the frequency was decreased in 25 kHz increments in the vicinity of the crossover. To aid the comparison among particle sizes, potentials are only shown in Figure 4 for $\omega/2\pi$ = 200, 300, 375, 500 and 1000 kHz.

In each plot, points correspond to potentials obtained from a Boltzmann inversion of measured particle histograms (i.e., eq 18), and lines correspond to potentials obtained by fitting eq 1 (evaluated at $z_m = h_m + a$) to the points using λ/f_{CM} as the only adjustable parameter at each frequency for each particle size. Table 3 lists all other parameters used for the theoretical potential energy profiles in Figure 4, which were obtained from independent measurements or literature results. Each potential was measured relative to its most probable position in the electrode gap. To compare measured and predicted potentials, potentials are shifted vertically so that all have the same reference potential energy at the middle of the electrode gap (i.e., $x = 0$).

Adjusting only values of λ/f_{CM} in eq 7 produces net predicted potentials in excellent agreement with the measured potentials in Figure 4. The positions of the minima within the electrode gap and the functional form of the measured potentials are in excellent agreement with predictions for both negative and positive f_{CM} values. It should be noted that potentials could not be measured exactly at the crossover frequency because the dipole−field interaction vanishes and particles diffuse out of the gap.

Table 3. Parameters Used to Fit eqs 1−7 to Measured Potential Energy Profiles for the PS Frequency Results in Figure 4[a]

parameter	equation	value
$2a$ (μm)[b]	3, 4, 6, 8, 12	3, 4, 5
$\varepsilon_m/\varepsilon_0$[c]	4, 8-11, 14,	78
κ^{-1} (nm)[d]	3, 13	30
$\zeta_p = \psi_p = \psi_w$ (mV)[e]	4, 13	−75
ρ_p (g/cm^3)[c]	6	1.055
ρ_m (g/cm^3)[c]	6	1
V_{pp} (mV)[f]	7	300
d_g (μm)[g]	7	25
$\omega/2\pi$ (kHz)[f]	10	100−1000

[a] The nondimensional dipole−field magnitudes, λ, were the only adjustable parameters, which are shown in Figure 5. [b] Parameter fixed using nominal manufacturer particle sizes. [c] Parameter fixed using handbook values.[38] [d] Parameter fixed using estimate from previous diffusion measurements.[14] [e] Parameter fixed using estimate from previous direct measurements.[39] [f] Parameter fixed using function generator input. [g] Parameter fixed by measuring with optical microscopy.

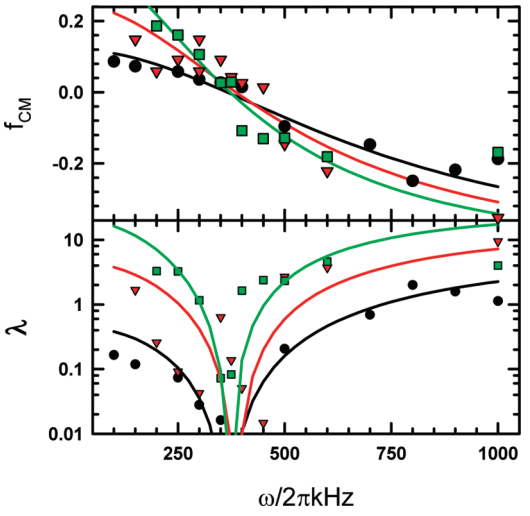

Figure 5. Values of f_{CM} vs ω (top) and λ vs ω (bottom) obtained by fitting eqs 1−7 to measured potential energy profiles in Figure 4. Theoretical curve fits for each particle size are obtained using eqs 8−14 with parameters reported in Table 4. Values are shown for 3 μm (black circles), 4 μm (red triangles), and 5 μm (green squares).

In addition to showing that the fit λ/f_{CM} captured the measured potentials in Figure 4, results in Figure 5 show the ability of available electrokinetic models to capture the frequency-dependent material properties that correspond to the fit λ and f_{CM} values. Figure 5 shows fit λ and f_{CM} values vs AC field frequency as points for each PS particle size and curve fits using eqs 8−14. Fit parameters are reported in Table 4. The fitting procedure used similar parameters to the silica particle analysis in Figure 3 (with parameters in Table 2). To correct for particle size and voltage biases observed in the silica-amplitude experiments, the fit values of λ obtained in Figure 4 (reported in Table 3) were divided by 0.8 before fitting eqs 8−14.

Table 4. Parameters Used to Fit eqs 8−14 to Measured λ Values for the PS-Frequency Results in Figure 5[a]

parameter	equation	value
$\varepsilon_p/\varepsilon_0$[b]	9	2.55
D (10^{-9} m^2 s^{-1})[b]	14	1.3
η (Pa−s)[b]	14	8.9×10^{-4}
m[c]	13	0.79
β^{-1} (nm)	13	**140, 280, 520**
σ_m (μS/cm)	10, 11, 13	**18.7, 11.8, 7.6**
K_n (nS)[c]	12	1.98, 2.34, 2.68
$\omega_C/2\pi$ (kHz)[c]	11	364, 385, 370
$\lambda_{fit}/\lambda_{predicted}$	- -	0.8

[a] The medium conductivity, σ_m, and slip length were the only adjustable parameters (shown in bold). [b] Parameter fixed using handbook values.[38] [c] Parameter fixed using equations.

As in the silica−amplitude measurements, σ_m was used an adjustable parameter. The PS-frequency experiments required β^{-1} in eq 13 as an additional fit parameter, which is a slip length that increases the surface conductance, K_n. The fit values of the medium conductivity were in the range σ_m = 8−19 μS/cm, consistent with a 0.1 mM NaCl solution and κ^{-1} = 30 nm. The fit "slip lengths" of β^{-1} = 140, 280, and 520 nm for PS particles with nominal diameters of $2a$ = 3, 4, and 5 μm correspond to nondimensional values of βa = 11, 7, and 5 for κa = 50, 67, and 83. The values of K_n including slip compared to those without slip are factors of 8, 15, and 26 times larger for the 3, 4, and 5 μm PS particles.

Slip lengths at 10−20% of the particle radii are excessively large, but appear to be needed in eq 13 to account for an order of magnitude increase in surface conductance compared to predictions without slip. Although we do not perform an exhaustive parametric analysis of the variables used to model f_{CM}, σ_p, and K_n in eqs 8−14, it is not obvious that any other parameters besides β^{-1} can be adjusted to account for the λ values that describe the potentials in Figure 4. For example, effects of particle size and voltage biases that effectively captured the silica−amplitude data have already been included in λ in eq 8. The remainder of the parameters contained in the electrokinetic models of f_{CM}, σ_p, and K_n in eqs 8−14 cannot be easily adjusted within their uncertainty and interdependency (e.g., κ^{-1} and σ_m) to account for the measured λ.

In contrast, the silica−amplitude data in Figures 2 and 3 are well described by eqs 8−14. Although the silica−amplitude results are limited to the negative f_{CM} case, this is a direct result of the low silica surface conductance, which does not allow for a crossover to a positive f_{CM} case. It is also the low silica surface conductance that does not require introduction of a slip length in eq 13. In contrast, the high surface conductance of PS particles that enables their crossover to positive f_{CM} values requires introduction of significant β^{-1} values in eq 13.

It is not likely that true hydrodynamic slip is being observed in the PS case, but rather that the second term in eq 13 is a placeholder for a different electrokinetic effect (e.g., "apparent slip"[34]) that produces the higher surface conductances. For example, it might be tempting to attribute the slip on the PS particles to their hydrophobic nature. However, measurements of slip lengths on hydrophobic surfaces are typically on the order of nanometers[35] rather than the ~100 nm lengths inferred from our measurements. It would be desirable to trace the differences observed between the silica and PS results and inferred surface conductances to real differences between physical roughness, molecular-scale structure (e.g., silica gel layers[36]), different charge groups (i.e., surface oxide vs sulfates groups), interfacial water structure, and so forth. However, in the absence of independent measurements of these effects, understanding the physical origin of the apparent slip on the PS particles is beyond the scope of the present study. It is also possible that more rigorous theories[37] could account for the PS results.

Aside from the anomalously high PS surface conductances, the silica and PS results together provide the first kT and fN scale measurements of single induced dipole-field interactions (as it vanishes near the crossover frequency). Both measurements confirm the spatial dependence of the induced dipole-field potential, and show that potential's magnitude can be accurately predicted for silica with no adjustable parameters and for PS with introduction of a single parameter (i.e., slip length). This provides a basis to manipulate and investigate single particles in inhomogeneous electric fields in a manner that minimally perturbs their equilibrium state (in contrast to strong fields and mechanical manipulation).

In Part II,[20] we use these single induced dipole−field interactions as a basis to understand how ensembles of particles behave in inhomogeneous electric fields, which is motivated by colloidal self-assembly problems. Because Part II requires consideration of dipole−dipole interactions in addition to dipole−field interactions, it is important to use the established dipole−field results obtained at infinite dilution in this work.

CONCLUSIONS

Our results demonstrate a new method to sensitively measure kT-scale induced dipole−field interactions as a function of particle size and field amplitude and frequency. For both silica and PS colloids, the magnitude and spatial dependence of measured interactions are well-described by theoretical dipole−field potentials by fitting a nondimensional induced dipole magnitude. While the silica dipole−field magnitudes are well-described by existing electrokinetic models of surface conductance, the PS dipole−field magnitudes suggest an anomalously high surface conductance that appears to require hydrodynamic slip using available models. The higher PS particle surface conductance is consistent with an observed frequency dependent crossover, which was not observed for silica particles due to their low surface conductance. Understanding the molecular and nanoscale electrokinetic mechanism(s) that produce the different surface conductance on the silica and PS particles is beyond the scope of the present work, but our findings and experimental approach might be useful for testing new models. The sensitive measurements and test of models of dipole−field interactions in this work provide the basis to understand dipole−dipole and multiparticle packing effects Part II.[20]

AUTHOR INFORMATION

Corresponding Author

*E-mail: mabevan@jhu.edu.

ACKNOWLEDGMENT

We acknowledge financial support provided by the National Science Foundation through a Cyber Enabled Discovery and

Innovation grant (CMMI-0835549) and an unsolicited grant (CBET-0932973), and the Air Force Office of Scientific Research (FA9550-08-1-0329).

REFERENCES

(1) Pohl, H. A. *Dielectrophoresis: the behavior of neutral matter in nonuniform electric fields*; Cambridge University Press: Cambridge, 1978; p xii.

(2) Jones, T. B. *Electromechanics of Particles*; Cambridge University Press: Cambridge, 1995; p 265.

(3) Morgan, H.; Green, N. G.,*AC electrokinetics: colloids and nanoparticles*; Research Studies Press: Philadelphia, 2003.

(4) Pethig, R.; Markx, G. H. Applications of dielectrophoresis in biotechnology. *Trends Biotechnol.* **1997**, *15* (10), 426–432.

(5) Pethig, R. Review Article---Dielectrophoresis: Status of the theory, technology, and applications. *Biomicrofluidics* **2010**, *4* (2), 022811.

(6) Zhou, H.; Preston, M. A.; Tilton, R. D.; White, L. R. Calculation of the electric polarizability of a charged spherical dielectric particle by the theory of colloidal electrokinetics. *J. Colloid Interface Sci.* **2005**, *285* (2), 845–856.

(7) Ermolina, I.; Morgan, H. The electrokinetic properties of latex particles: comparison of electrophoresis and dielectrophoresis. *J. Colloid Interface Sci.* **2005**, *285* (1), 419–428.

(8) Basuray, S.; Chang, H.-C. Induced dipoles and dielectrophoresis of nanocolloids in electrolytes. *Phys. Rev. E* **2007**, *75* (6), 060501.

(9) Zhao, H. On the effect of hydrodynamic slip on the polarization of a nonconducting spherical particle in an alternating electric field. *Phys. Fluids* **2010**, *22* (7), 072004–15.

(10) Saville, D. A.; Bellini, T.; Degiorgio, V.; Mantegazza, F. An extended Maxwell--Wagner theory for the electric birefringence of charged colloids. *J. Chem. Phys.* **2000**, *113* (16), 6974–6983.

(11) O'Konski, C. T. Electric Properties of Macromolecules. V. Theory of Ionic Polarization in Polyelectrolytes. *J. Phys. Chem.* **1960**, *64* (5), 605–619.

(12) Fernandes, G. E.; Beltran-Villegas, D. J.; Bevan, M. A. Interfacial Colloidal Crystallization via Tunable Hydrogel Depletants. *Langmuir* **2008**, *24*, 10776–10785.

(13) Fernandes, G. E.; Beltran-Villegas, D. J.; Bevan, M. A. Spatially Controlled Reversible Colloidal Self-Assembly. *J. Chem. Phys.* **2009**, *131*, 134705.

(14) Juarez, J. J.; Bevan, M. A. Electric Field Induced Colloidal Interactions and Equilibrium Microstructures. *J. Chem. Phys.* **2009**, *131*, 134704.

(15) Wang, X. B.; Huang, Y.; Burt, J. P. H.; Markx, G. H.; Pethig, R. Selective Dielectrophoretic Confinement of Bioparticles in Potential-Energy Wells. *J. Phys. D: Appl. Phys.* **1993**, *26* (8), 1278–1285.

(16) Docoslis, A.; Alexandridis, P. One-, two-, and three-dimensional organization of colloidal particles using nonuniform alternating current electric fields. *Electrophoresis* **2002**, *23* (14), 2174–2183.

(17) Abe, M.; Orita, M.; Yamazaki, H.; Tsukamoto, S.; Teshima, Y.; Sakai, T.; Ohkubo, T.; Momozawa, N.; Sakai, H. Three-Dimensional Arrangements of Polystyrene Latex Particles with a Hyperbolic Quadruple Electrode System. *Langmuir* **2004**, *20* (12), 5046–5051.

(18) Wei, M.-T.; Junio, J.; Ou-Yang, H. D. Direct measurements of the frequency-dependent dielectrophoresis force. *Biomicrofluidics* **2009**, *3* (1), 012003.

(19) Bevan, M. A.; Eichmann, S. L. Optical Microscopy Measurements of kT-Scale Colloidal Interactions. *Curr. Opin. Colloid Interface Sci.* **2011**, *16* (2), 149–157.

(20) Juarez, J. J.; Liu, B.; Cui, J.; Bevan, M. A. kT-Scale Colloidal Interactions in High Frequency Inhomogeneous AC Electric Fields. II. Concentrated Ensembles. *Langmuir* **2011**, in press; doi: 10.1021/la2014804.

(21) Russel, W. B.; Saville, D. A.; Schowalter, W. R. *Colloidal Dispersions*; Cambridge University Press: New York, 1989.

(22) Jones, T. B.; Washizu, M. Equilibria and dynamics of DEP-levitated particles: multipolar theory. *J. Electrostatics* **1994**, *33* (2), 199–212.

(23) Adriani, P. M.; Gast, A. P. A microscopic model of electrorheology. *Phys. Fluids* **1988**, *31* (10), 2757–2768.

(24) Khair, A. S.; Squires, T. M. The influence of hydrodynamic slip on the electrophoretic mobility of a spherical colloidal particle. *Phys. Fluids* **2009**, *21* (4), 042001–14.

(25) Hinch, E. J.; Sherwood, J. D.; Chew, W. C.; Sen, P. N. Dielectric response of a dilute suspension of spheres with thin double layers in an asymmetric electrolyte. *J. Chem. Soc., Faraday Trans. 2* **1984**, *80* (5), 535–551.

(26) O'Brien, R. W. The high-frequency dielectric dispersion of a colloid. *J. Colloid Interface Sci.* **1986**, *113* (1), 81–93.

(27) Wu, H.-J.; Everett, W. N.; Anekal, S. G.; Bevan, M. A. Mapping Patterned Potential Energy Landscapes with Diffusing Colloidal Probes. *Langmuir* **2006**, *22*, 6826–6836.

(28) Crocker, J. C.; Grier, D. G. Methods of Digital Video Microscopy for Colloidal Studies. *J. Colloid Interface Sci.* **1996**, *179*, 298–310.

(29) Bahukudumbi, P.; Everett, W. N.; Beskok, A.; Huff, G. H.; Lagoudas, D.; Ounaies, Z.; Bevan, M. A. Colloidal Microstructures, Transport, and Impedance Properties within Interfacial Microelectrodes. *Appl. Phys. Lett.* **2007**, *90*, 224102.

(30) Bike, S. G.; Prieve, D. C. Measurements of Double-Layer Repulsion for Slightly Overlapping Counterion Clouds. *Int. J. Multiphase Flow* **1990**, *16* (4), 727–740.

(31) Wu, H. J.; Bevan, M. A. Direct Measurement of Single and Ensemble Average Particle-Surface Potential Energy Profiles. *Langmuir* **2005**, *21* (4), 1244–1254.

(32) Wu, H.-J.; Pangburn, T. O.; Beckham, R. E.; Bevan, M. A. Measurement and Interpretation of Particle−Particle and Particle−Wall Interactions in Levitated Colloidal Ensembles. *Langmuir* **2005**, *21* (22), 9879–9888.

(33) Wu, H.; Shah, S.; Beckham, R. E.; Meissner, K.; Bevan, M. A. Resonant Effects in Evanescent Wave Scattering of Polydisperse Colloids. *Langmuir* **2008**, *24*, 13790–13795.

(34) Lauga, E.; Brenner, M. P.; Stone, H. A. *Microfluidics: The no-slip boundary condition*; Springer: Berlin, 2006.

(35) Bouzigues, C. I.; Tabeling, P.; Bocquet, L. Nanofluidics in the Debye Layer at Hydrophilic and Hydrophobic Surfaces. *Phys. Rev. Lett.* **2008**, *101* (11), 114503.

(36) Škvarla, J. Hard versus Soft Particle Electrokinetics of Silica Colloids. *Langmuir* **2007**, *23* (10), 5305–5314.

(37) Zhou, H.; Preston, M. A.; Tilton, R. D.; White, L. R. Calculation of the dynamic impedance of the double layer on a planar electrode by the theory of electrokinetics. *J. Colloid Interface Sci.* **2005**, *292* (1), 277–289.

(38) Lide, D. R. *CRC Handbook of Chemistry and Physics*; CRC Press: New York, 2000; Vol 80.

(39) Bevan, M. A. Effect of Adsorbed Polymer on the Interparticle Potential. PhD Dissertation, Carnegie Mellon University, Pittsburgh, PA, 1999.